JACS
JOURNAL OF THE AMERICAN CHEMICAL SOCIETY
pubs.acs.org/JACS
Article

Photocatalytic Dinitrogen Fixation with Water on Bismuth Oxychloride in Chloride Solutions for Solar-to-Chemical Energy Conversion

Yasuhiro Shiraishi,* Masaki Hashimoto, Kiyomichi Chishiro, Kenta Moriyama, Shunsuke Tanaka, and Takayuki Hirai

Cite This: https://dx.doi.org/10.1021/jacs.0c01683
Read Online

ABSTRACT: Ammonia is an indispensable chemical. Photocatalytic NH_3 production via dinitrogen fixation using water by sunlight illumination under ambient conditions is a promising strategy, although previously reported catalysts show insufficient activity. Herein, we showed that ultraviolet light irradiation of a semiconductor, bismuth oxychloride with surface oxygen vacancies (BiOCl-OVs), in water containing chloride anions (Cl^-) under N_2 flow efficiently produces NH_3. The surface OVs behave as the N_2 reduction sites by the photoformed conduction band electrons. The valence band holes are consumed by self-oxidation of interlayer Cl^- on the catalyst. The hypochloric acid (HClO) formed absorbs ultraviolet light and undergoes photodecomposition into O_2 and Cl^-. These consecutive photoreactions produce NH_3 with water as the electron donor. The Cl^- in solution compensates for the removed interlayer Cl^- and inhibits catalyst deactivation. Simulated sunlight illumination of the catalyst in seawater stably generates NH_3 with 0.05% solar-to-chemical conversion efficiency, thus exhibiting significant potential of the seawater system for artificial photosynthesis.

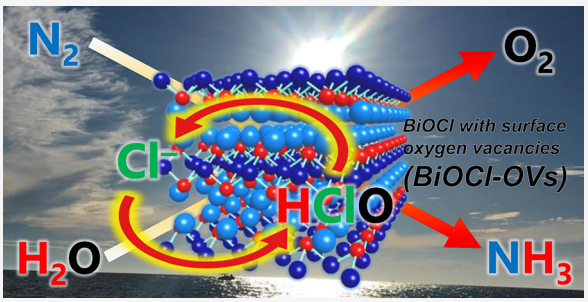

INTRODUCTION

Ammonia (NH_3), an indispensable chemical in modern society,[1] has attracted much attention as an energy carrier[2] and a component of an NH_3/O_2 fuel cell for electricity generation.[3] The industrial process for manufacturing NH_3 needs high pressure and high temperature conditions with large amounts of H_2.[4] A new N_2 fixation process that can be operated under milder reaction conditions is necessary, and in this respect, the photocatalytic process is promising because water can be used as a reductant under ambient reaction conditions.[5] In this method, sunlight irradiation of powder photocatalysts suspended in water produces valence band holes (VB h^+) for water oxidation (eq 1) and conduction band electrons (CB e^-) for N_2 reduction (eq 2). These redox reactions result in the formation of NH_3 with a large free energy gain (eq 3).[6] The photocatalytic N_2 fixation, along with overall water splitting (eq 4)[7−9] and H_2O_2 production (eq 5),[10−12] is therefore a potentially new artificial photosynthesis system.

$$2H_2O + 4h^+ \rightarrow O_2 + 4H^+ \quad (1)$$

$$N_2 + 6H^+ + 6e^- \rightarrow 2NH_3 \quad (2)$$

$$1/2N_2 + 3/2H_2O \xrightarrow{h\nu} NH_3 + 3/4O_2 \ (\Delta G^\circ = 339\ \mathrm{kJ\ mol^{-1}}) \quad (3)$$

$$H_2O \xrightarrow{h\nu} H_2 + 1/2O_2 \ (\Delta G^\circ = 237\ \mathrm{kJ\ mol^{-1}}) \quad (4)$$

$$H_2O + 1/2O_2 \xrightarrow{h\nu} H_2O_2 \ (\Delta G^\circ = 117\ \mathrm{kJ\ mol^{-1}}) \quad (5)$$

Early studies on photocatalytic N_2 fixation have been focused primarily on TiO_2-based catalysts.[13] Recent rapid progress in this field have demonstrated that N_2 fixation with water can be promoted on several types of powder photocatalysts[5,14] composed of noble metals,[15,16] binary or ternary metal oxides,[17−19] metal hydroxides,[20] metal sulfides,[21] metal chalcogels,[22] and carbonaceous materials,[23−25] where noble-metal-free inexpensive photocatalysts[17−25] are considered to be the most practical system for large-scale applications. Although several systems have been proposed, many of them have problems where it is unclear whether N_2 is the source of NH_3 and whether O_2 and NH_3 are generated quantitatively (eq 3). Noble-metal-free photocatalysts that efficiently catalyze both water oxidation and N_2 reduction are necessary.

Received: February 11, 2020

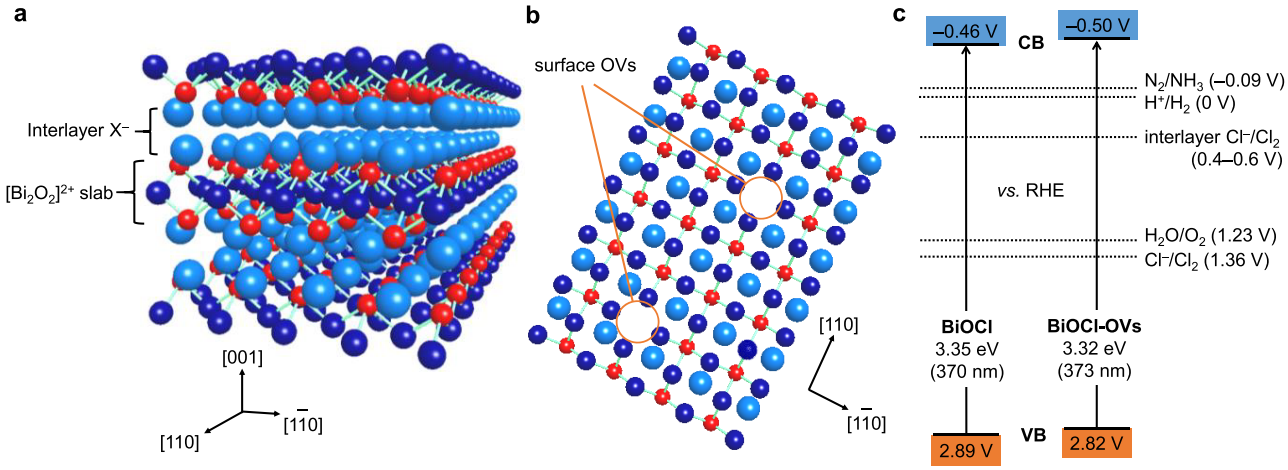

Figure 1. (a) Crystal and (b) surface structures of BiOX-OVs, where the Bi, O, and halide ions are denoted by blue, red, and cyan spheres, respectively. (c) Electronic band structure of BiOCl and BiOCl-OVs. The potentials for N_2/NH_3 and Cl^-/Cl_2 are from refs 15 and 54, respectively, while that for interlayer Cl^-/Cl_2 is based on the data in Figure 3.

N_2 fixation occurs via the N_2 reduction (eq 2);[5] hence, highly active N_2 reduction site is necessary. Recently, we found that TiO_2 with surface oxygen vacancies (OVs) reduces N_2 using water under ultraviolet light and efficiently produce NH_3 with a solar-to-chemical conversion (SCC) efficiency of 0.02%.[26] Several spectroscopic analysis indicate that the Ti^{III} sites adjacent to the OVs behave as the N_2 reduction sites, although an alternative mechanism involving adventitious carbons on the TiO_2 surface has been proposed on the basis of X-ray photoelectron spectroscopy (XPS) and density functional theory calculations.[27,28] Therefore, creating surface defects may become a promising strategy for N_2 fixation. Another rate-determining step is water oxidation by the VB h^+ (eq 1), which is a thermodynamically unfavorable multi-electron reaction.[29,30] Semiconductor photocatalysts with defective surface sites for N_2 reduction and high activity for water oxidation are necessary for efficient N_2 reduction with water as the electron donor.

Our strategy is the use of bismuth oxyhalides [BiOX (X = Cl, Br, I)], which are nontoxic, inexpensive, and environmentally friendly semiconductors.[31,32] As shown in Figure 1a, BiOX have a layered tetragonal matlockite structure, characterized by $[Bi_2O_2]^{2+}$ slabs interleaved by double slabs of halogen anions (X^-). Recent reports revealed that BiOX with surface OVs (BiOX-OVs), which behave as the N_2 reduction sites (Figure 1b),[33] exhibit high activity for photocatalytic N_2 fixation.[34−37] The BiOX photoexcited in water are, however, readily deactivated by self-decomposition because of their characteristic band structures. In the case of BiOCl-OVs, the density of states near its VB maximum mainly consists of Cl 3p orbitals because Cl has a lower electronegativity than O. The VB h^+ therefore preferentially oxidizes the interlayer Cl^- (eq 6) instead of water (eq 1).[38] This leads to self-oxidation (eq 7)[39] and self-reduction (eq 8)[40] of the lattice Bi^{III}, creating an inactive surface. Promoting stable water oxidation on BiOX-OVs while suppressing self-deactivation is a key to efficient N_2 fixation.

$$2Bi^{III}OCl + 2h^+ \rightarrow 2Bi^{III}O^+ + Cl_2 \quad (6)$$

$$2Bi^{III}O^+ + 2H_2O + 2h^+ \rightarrow Bi^{III}Bi^{V}O_4 + 4H^+ \quad (7)$$

$$Bi^{III}O^+ + 2H^+ + 3e^- \rightarrow Bi^0 + H_2O \quad (8)$$

Herein, we demonstrate that photocatalysis by BiOCl-OVs in chloride solutions such as "seawater" solves the depletion of the interlayer Cl^-. We found that ultraviolet light irradiation of BiOCl-OVs in water containing chloride anions (Cl^-) under N_2 flow stably produces NH_3 with water. The surface OVs behave as the sites of N_2 reduction by the CB e^- (eq 2). The VB h^+ are consumed by self-oxidation of interlayer Cl^-, producing Cl_2 (eq 6). The Cl^- in solution compensates for the removed interlayer Cl^- and prevents the subsequent reactions (eqs 7 and 8), thus suppressing catalyst deactivation. As expressed by eq 9, the Cl_2 photoformed in water is in equilibrium with hypochloric acid (HClO).[41] It absorbs ultraviolet light and undergoes photodecomposition to O_2 and Cl^- (eq 10).[42−44] The Cl^- compensation and photodecomposition of HClO therefore stably and quantitatively produce NH_3 with water as the electron donor (eq 3).

$$Cl_2 + H_2O \rightleftharpoons HClO + H^+ + Cl^-(pK_a = 1.4) \quad (9)$$

$$HClO \xrightarrow{h\nu} 1/2O_2 + H^+ + Cl^- \quad (10)$$

RESULTS AND DISCUSSION

Characterization of Catalysts. BiOCl (with perfect stoichiometry) or BiOCl-OVs was prepared by a solvothermal method with $Bi(NO_3)_3{\cdot}5H_2O$ and KCl in water[34] or ethylene glycol,[35] respectively. Scanning electron microscopy (SEM) observation of BiOCl and BiOCl-OVs (Figure S1) shows platelike particles with ∼1 μm and ∼0.3 μm diameters, respectively. N_2 adsorption/desorption analysis of both catalysts shows type III isotherms (Figure S2), and the calculated surface areas of BiOCl and BiOCl-OVs are only 8.4 and 16.1 $m^2\ g^{-1}$, respectively, which are indicative of nonporous particles. Both catalysts absorb light at $\lambda < 370$ nm with a similar bandgap energy of ∼3.3 eV (Figure S3). Electrochemical Mott−Schottky plots of the catalysts (Figure S4) exhibit n-type responses with similar flat-band potentials [approximately − 0.50 V vs reversible hydrogen electrode (RHE)]. These data clearly indicate that BiOCl and BiOCl-OVs have similar electronic band structures (Figure 1c). X-ray diffraction (XRD) of the catalysts (Figure S5) indicates that all of the peaks can be indexed to a tetragonal BiOCl structure (JCPDS card 06-0249).

https://dx.doi.org/10.1021/jacs.0c01683
J. Am. Chem. Soc. XXXX, XXX, XXX−XXX

Table 1. Compositions of BiOCl and BiOCl-OVs

entry	catalyst	status[a]	elemental composition/%[b]			composition of Bi species/%[c]			
			Bi	O	Cl	Bi^{V}	Bi^{III}	Bi^{II}	Bi^{0}
1	BiOCl	fresh	33.4	33.3	33.3	4.1	95.9	<0.1	<0.1
2	BiOCl-OVs	fresh	38.9	27.8	33.3	5.4	84.8	9.8	<0.1
3	BiOCl-OVs	after reaction in pure water	53.6	24.0	22.3	25.2	50.0	25.7	4.1
4	BiOCl-OVs	after reaction in KCl solution (pH 1.0)	39.0	28.4	32.6	8.1	81.7	10.2	<0.1

[a]Photoreaction condition: solution (0.1 L), catalyst (0.2 g), N_2 (0.3 L min^{-1}), λ > 300 nm (Xe lamp, intensity at 300−400 nm: 40.7 W m^{-2}), temperature (303 K), and photoirradiation time (24 h). [b]Determined from the XPS peak areas with atomic sensitivity factors (Bi 4f, 1.00; Cl 2p, 7.31; O 1s, 6.34). [c]Calculated from the XPS (Bi 4f) peak areas.

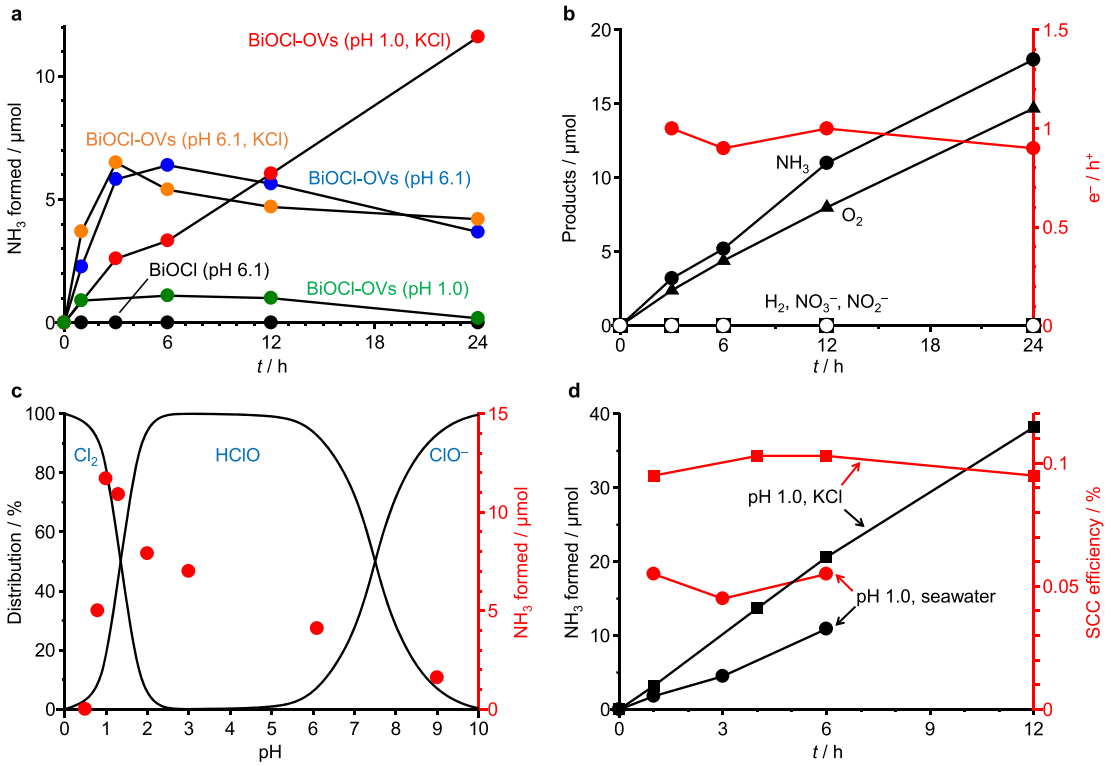

Figure 2. (a) Amounts of NH_3 produced during the photoreactions [conditions: solution (0.1 L), catalyst (0.2 g), N_2 (0.3 L min^{-1}), λ > 300 nm (Xe lamp, intensity at 300−400 nm: 40.7 W m^{-2}), and temperature (303 K)]. (b) The product amounts and e^-/h^+ balance {= $[NH_3] \times 3/([O_2] \times 4)$} during the photoreaction (Xe lamp) on BiOCl-OVs in 550 mM KCl solution (pH 1.0) using a closed gas circulation system (0.04 MPa N_2). (c) Mole fraction distributions of Cl_2, HClO, and ClO^- in the solution and amount of NH_3 formed on BiOCl-OVs by photoirradiation (Xe lamp) for 24 h in 550 mM KCl solution with different pH values. (d) Amounts of NH_3 formed and SCC efficiency under simulated sunlight (1 sun), where the light intensity at 300−400 nm is 291 W m^{-2}.

XPS spectrum of BiOCl-OVs at the Bi 4f level (Figure S6) shows two components assigned to lattice Bi^{III} (157.2 and 162.5 eV) and Bi^{II} adjacent to the surface OVs (156.6 and 161.9 eV).[45] As summarized in Table 1, BiOCl does not contain Bi^{II} but BiOCl-OVs contain 9.8% Bi^{II}, confirming the presence of surface OVs. XPS spectra of both catalysts at the O 1s level (Figure S7) exhibit two components assigned to lattice O (528.1 eV) and surface −OH (529.4 eV), and the spectra at the Cl 2p level (Figure S8) show components assigned to interlayer Cl^- (196.0 and 197.5 eV).[46] The elemental compositions of the catalyst surfaces (Bi, O, Cl) were determined from the XPS peak areas using the individual atomic sensitivity factors (Table 1).[47] The almost 1:1:1 Bi:O:Cl composition of BiOCl agrees with the theoretical stoichiometry. The O composition of BiOCl-OVs (28%) is lower than that of BiOCl (33%), confirming the formation of surface OVs. Electron spin resonance (ESR) spectrum of BiOCl-OVs at 77 K (Figure S9) exhibits a Lorentzian line attributable to the unpaired electron on Bi^{II} adjacent to the surface OVs,[45] whereas that of BiOCl does not show such a signal. These data clearly suggest that BiOCl-OVs contains surface OVs.

Photocatalysis in Pure Water. N_2 fixation on the BiOCl or BiOCl-OVs catalyst in pure water is ineffective. Reactions were carried out by photoirradiation (λ > 300 nm) of water (0.1 L) containing BiOCl or BiOCl-OVs (0.2 g) by a Xe lamp[48] (Figure S10) under N_2 flow at 303 K. Note that the pH of the solutions during the reaction is ∼6.1, and the generated NH_3 exists in the protonated NH_4^+ form (pK_a 9.3).[49] Figure 2a shows the time profile for the amount of NH_3 formed. BiOCl (black) does not produce NH_3. In contrast, BiOCl-OVs (blue) produces NH_3, indicating that the surface OVs indeed act as the N_2 reduction sites.[33] The NH_3 amount increases at the early stage but decreases with time. This decrease originates

https://dx.doi.org/10.1021/jacs.0c01683
J. Am. Chem. Soc. XXXX, XXX, XXX−XXX

from the self-deactivation of the catalyst and subsequent decomposition of the NH_3 formed. The VB h^+ photoformed on the catalyst are consumed by oxidation of interlayer Cl^- (eq 6).[38] This Cl^- removal leads to catalyst deactivation by subsequent self-oxidation and self-reduction reactions (eqs 7 and 8). The Cl^- removal is confirmed by XPS (Table 1, entry 3). The Cl composition of BiOCl-OVs (33%) decreases to 22% after the photoreaction. The Bi 4f XPS spectrum of the recovered catalyst (Figure S6) shows a Bi^V component (158.3 and 163.3 eV)[39] formed via oxidation of Bi^{III} by the VB h^+ (eq 7) and Bi^0 component (155.8 and 161.2 eV)[40] formed via reduction of Bi^{III} by the CB e^- (eq 8). In addition, as shown in Figure S3, the recovered catalyst exhibits a broad absorption at $\lambda > 350$ nm assigned to the Bi^0 species.[50] These data indicate that Cl^- removal in BiOCl-OVs leads to a loss of charge balancing and promotes subsequent self-oxidation and self-reduction reactions, leading to the self-deactivation of the catalyst.

Self-deactivation in pure water was further confirmed by cyclic voltammetry (CV) of BiOCl-OVs measured on a glassy carbon electrode in 1.0 M Na_2SO_4 under N_2 flow (Figure 3a).

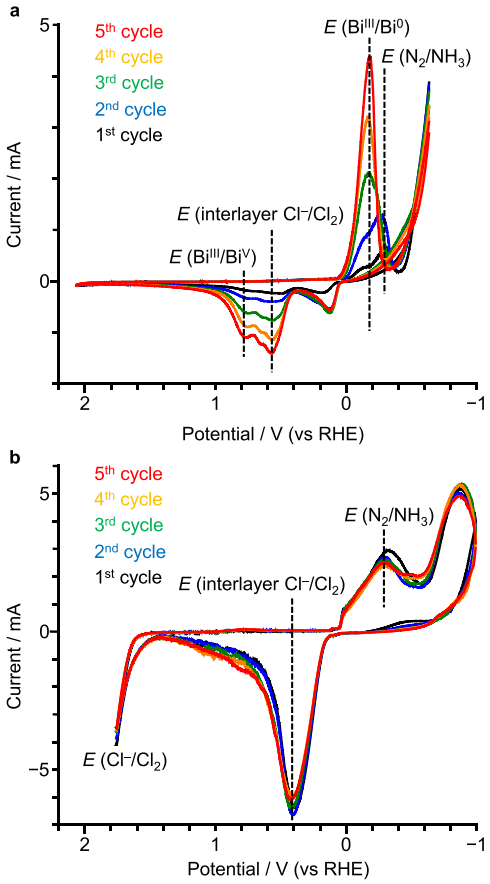

Figure 3. CV curves of BiOCl-OVs measured in (a) 1.0 M Na_2SO_4 solution (pH 6.1) and (b) 550 mM KCl solution (pH 1.0) under N_2 bubbling with a sweep speed of 0.1 V/sec.

Early cycles show an anodic current for oxidation of interlayer Cl^- (+0.57 V vs RHE) and a cathodic current for N_2 reduction (−0.30 V). Note that an anodic current for water oxidation does not appear, clearly indicating that the catalyst is inactive for water oxidation.[38] Continuous cycles promote Bi^{III}/Bi^V oxidation (+0.78 V) and Bi^{III}/Bi^0 reduction (−0.19 V),[51] along with almost complete inhibition of N_2 reduction. This indicates that oxidation of interlayer Cl^- triggers irreversible self-oxidation and -reduction reactions, resulting in catalyst deactivation. As shown in Table S1, entry 1, the BiOCl-OVs recovered after the photoreaction in pure water [Figure 2a (blue)], when reused for further reactions, shows decreased activity, confirming the catalyst deactivation.

The Cl_2 formed by the self-oxidation of interlayer Cl^- is in equilibrium with HClO (eq 9),[41] which exists mainly at neutral pH. Therefore, as expressed by eq 11, HClO oxidizes the photoformed NH_3, which then decomposes to N_2 and H_2O. This decomposition accounts for the decreased NH_3 amount during the reaction [Figure 2a (blue)]. The solution recovered during the photoirradiation of BiOCl-OVs in pure water exhibits characteristic absorption bands at around 240 and 300 nm assigned to HClO (Figure S11).[42] In addition, NH_3, when stirred in a NaClO solution (pH 6.1) in the dark, indeed undergoes decomposition (Figure S12). These data suggest that photoexcitation of BiOCl-OVs in pure water leads to self-deactivation triggered by oxidation of the interlayer Cl^- and decomposition of the formed NH_3 via oxidation by HClO. These negative effects result in inefficient NH_3 formation [Figure 2a (blue)].

$$2NH_4^+ + 3HClO \rightarrow N_2 + 5H^+ + 3Cl^- + 3H_2O \qquad (11)$$

Photocatalysis in Acidic Cl^- Solution. Photoexcitation of BiOCl-OVs in an acidic solution containing Cl^- suppresses deactivation of the catalyst and decomposition of the NH_3 formed, leading to a stable NH_3 production. Photoreaction was performed in a KCl solution at pH 1.0 with BiOCl-OVs under N_2 flow. The Cl^- concentration in the solution was set to 550 mM, which is the same as that in seawater, and its pH was adjusted with $HClO_4$ to maintain the Cl^- concentration.[44] As shown in Figure 2a (red), the NH_3 amount increases linearly with time, indicating that the system suppresses deactivation of the catalyst and decomposition of the NH_3 formed. Note that, as shown in Figure 2a, photoreaction in either a neutral KCl solution (pH 6.1) (orange) or acidic solution (pH 1.0) without KCl (green) is ineffective, indicating that an acidic Cl^- solution is necessary. Also note that, as shown in Table S1, entry 2, photoirradiation of BiOCl in an acidic KCl solution does not produce NH_3, again confirming that the OVs behave as the N_2 reduction sites. In addition, as shown by entries 3 and 4, the dark reaction or irradiation of $\lambda > 420$ nm light, which is not absorbed by the catalyst, does not promote the reaction. Furthermore, the catalyst recovered after the photoreaction in an acidic Cl^- solution, when reused 5 times for further reactions, exhibits almost the same activity as the fresh one (entry 5), indicating that the catalyst is reusable without loss of activity. During the reaction, UV−visible spectroscopy[52] or ion chromatography analysis does not detect hydrazine, NO_3^-, or NO_2^-, indicating that NH_3 is the sole product from N_2.

During the photoreaction, the interlayer Cl^- removed from the catalyst is compensated by the Cl^- in the solution, suppressing catalyst deactivation. As shown in Table 1 (entry 4), the Cl composition of BiOCl-OVs recovered after the reaction scarcely changes, indicative of successful Cl^- compensation. In addition, the Bi 4f XPS spectrum of the recovered catalyst scarcely shows an increase in the Bi^V or Bi^0 component (Figure S6). In addition, as shown in Figure S3, the recovered catalyst shows absorption spectrum similar to that of the fresh one, where a broad absorption at $\lambda > 350$ nm

https://dx.doi.org/10.1021/jacs.0c01683
J. Am. Chem. Soc. XXXX, XXX, XXX−XXX

assigned to Bi^0 species[50] scarcely appears. These data indicate that Cl^- compensation by the solution suppresses self-oxidation and -reduction reactions (eqs 7 and 8), thus inhibiting catalyst deactivation. Note that SEM images and XRD pattern of the recovered catalyst are similar to those of the fresh one (Figures S1 and S5), suggesting that the morphology and optical properties of the catalyst scarcely change. In addition, at this acidic pH (1.0), the HClO concentration decreases because of the displacement of the equilibrium with Cl_2 as expressed by eq 9. As shown in Figure S12, NH_3 stirred in a NaClO solution (pH 1.0) scarcely decomposes, indicating that the NH_3 decomposition by HClO is suppressed in an acidic solution. These findings clearly suggest that photoexcitation of BiOCl-OVs in an acidic Cl^- solution suppresses deactivation of the catalyst and decomposition of the NH_3 formed, thus promoting efficient NH_3 formation.

As shown in Table S1, entry 6, photoreaction on BiOCl-OVs under Ar gas does not produce NH_3, suggesting that the N source of NH_3 is the N_2 gas. To further confirm this, photoreaction was carried out using isotope-labeled $^{15}N_2$. A KCl solution (pH 1.0) containing BiOCl-OVs was photoirradiated with $^{14}N_2$ or $^{15}N_2$ (0.13 MPa) for 36 h, where the amounts of NH_3 formed from $^{14}N_2$ and $^{15}N_2$ were similar (74 and 72 μM, respectively). The NH_3 formed was converted by the indophenol assay.[24,26] The resulting solution with the distinctive indophenol absorption band at 630 nm was analyzed by liquid chromatography−mass spectrometry (Figure S13). The $^{14}N_2$ sample exhibits an indophenol anion peak (m/z 198), and the $^{15}N_2$ sample exhibits a very strong ^{15}N-labeled anion peak (m/z 199), confirming N_2 as the N source of NH_3.

Photocatalytic Properties in Acidic Cl^- Solution. Upon photoexcitation of BiOCl-OVs in an acidic Cl^- solution, "water" acts as the electron donor and promotes stoichiometric N_2 reduction. Oxidation of interlayer Cl^- by the VB h^+ (eq 6) produces HClO by driving the forward reaction in eq 9. HClO absorbs ultraviolet light and is decomposed to O_2 and Cl^- (eq 10).[42−44] These consecutive reactions therefore consume the VB h^+ by water oxidation. The direct electron donor is the interlayer Cl^-, and the photodecomposition of HClO is the reaction to regenerate Cl^- with water as an electron donor, where HClO acts as a photoredox substrate to produce O_2 and Cl^-. As shown in Figure S14, photoirradiation of a NaClO solution (pH 1.0) under Ar indeed produces O_2, confirming the photodecomposition of HClO. During the photoreaction on BiOCl-OVs in a KCl solution (pH 1.0) under N_2 flow (Figure 2a, red), the outlet gas was bubbled through pure water. The pH of the solution does not change during the reaction, indicating that Cl_2 is not removed as a gas. The amount of HClO formed in the solution was determined by an absorption spectroscopy with a DPD (N,N-dimethyl-p-phenylenediamine) reagent.[53] The DPD assay of the solutions shows absorption bands assigned to the oxidized form of DPD (Figure S15). As shown in Figure S16, the HClO formed is less than 1 μmol during the photoreaction, which are much smaller than the amounts of NH_3 formed. This indicates that HClO formed via the oxidation of interlayer Cl^- by the VB h^+ is readily photodecomposed into O_2 and Cl^-. Stoichiometric water oxidation and N_2 reduction on BiOCl-OVs in a KCl solution (pH 1.0) are confirmed by photoreaction in a closed gas circulation system (0.04 MPa N_2). Figure 2b shows the time course for the product amounts during the reaction. The NH_3 and O_2 amounts increase almost linearly, where H_2 is not formed over the entire reaction time. The e^-/h^+ balance determined by the amounts of NH_3 and O_2 formed {= $[NH_3] \times 3/([O_2] \times 4)$} is almost 1. These results suggest that O_2 evolution by photodecomposition of HClO (eq 10) occurs very rapidly, and hence, N_2 reduction occurs stoichiometrically with water as the electron donor (eq 3). It must be noted that NO_2^- or NO_3^- is not produced during the reaction (Figure 2b). To further confirm this, a KCl solution (pH 1.0, 50 mL) containing 50 μmol NH_3 and BiOCl-OVs catalyst (0.1 g) was photoirradiated under O_2 (0.13 MPa). The NH_3 amount scarcely changes even after 24 h of photoreaction. This clearly indicates that subsequent oxidation of the formed NH_3 by the VB h^+ with the photoformed O_2 does not occur in the present system.

Figure 3b shows the CV curve of BiOCl-OVs measured in an acidic KCl solution (pH 1.0). The negative current for the self-oxidation of interlayer Cl^- (+0.41 V vs RHE) and positive current for N_2 reduction (−0.30 V) are steadily observed, and Bi^{III}/Bi^{V} oxidation and Bi^{III}/Bi^0 reduction do not occur. This clearly indicates that the interlayer Cl^- removed by oxidation by VB h^+ are successfully compensated by the Cl^- in solution. Almost no current for the Bi^{III}/Bi^{V} oxidation in the CV chart (0.1 V/sec) implies that Cl^- in solution may be compensated at least 5 s after the removal of interlayer Cl^-. This suppresses subsequent self-oxidation and -reduction reactions (eqs 7 and 8) and stably promotes N_2 reduction. Note that self-oxidation of interlayer Cl^- (+0.41 V vs RHE) occurs at a more negative potential compared with oxidation of Cl^- in the bulk solution (>+1.5 V vs RHE), as shown in Figure 1c.[54] This indicates that the VB h^+ photoformed on BiOCl-OVs are consumed by self-oxidation of the interlayer Cl^-, whereas the Cl^- in solution is not oxidized.

Photocatalytic Performance. The pH of the Cl^- solution is crucial for efficient N_2 fixation. Figure 2c shows the amounts of NH_3 formed by photoirradiation of BiOCl-OVs for 24 h in KCl solutions with different pH values and mole fraction distribution of the Cl_2, HClO, and ClO^- species in the solution. At pH > 3, HClO is the major species in the solution and decomposes the NH_3 formed (eq 11), resulting in low efficiency for NH_3 formation. At pH < 3, the HClO concentration decreases by equilibrium displacement, which suppresses NH_3 decomposition and consequently enhances NH_3 formation. The highest activity is achieved at pH 1.0, but a lower pH significantly decreases the activity. This is because, under strongly acidic condition, BiOCl is decomposed to Bi^{III} and dissolved to the solution (eq 12).[55] This decomposition does not occur at pH 1.0, but occurs at lower pH. Figure S17 shows photographs of the solutions with different pH after stirring with BiOCl-OVs for 1 h. At pH 6.1 and 1.0, almost all of the powders remain in the solutions. In contrast, 85% of the powders are dissolved at pH 0.7, and all of them are dissolved at pH 0.5. These findings indicate that an acidic Cl^- solution with pH ∼ 1.0 is the best solvent for N_2 fixation. Note that, as shown in Table S1, entries 7 and 8, the use of HCl or H_2SO_4 in place of $HClO_4$ to adjust the pH of the solution (= 1) produces a similar amount of NH_3 to that obtained with $HClO_4$ (entry 5), indicating that the acid used scarcely affects the N_2 fixation activity.

$$Bi^{III}OCl + 2H^+ \rightarrow Bi^{III} + Cl^- + H_2O \quad (12)$$

As shown in Table S1, entry 9, photoreaction under air flow gives a small amount of NH_3, but the recovered catalyst, when

https://dx.doi.org/10.1021/jacs.0c01683
J. Am. Chem. Soc. XXXX, XXX, XXX−XXX

reused for photoreaction under N_2 flow, successfully produces N_2. This indicates that, under air flow, preferential O_2 adsorption or reduction suppresses N_2 reduction, where the surface OVs are not irreversibly deactivated. Furthermore, photoreaction in a closed N_2 atmosphere (0.13 MPa) also gives a small amount of NH_3 (entry 10) because the photoformed O_2 (eq 1) may suppress N_2 reduction. Continuous N_2 flow to remove O_2 from the system is therefore necessary for efficient N_2 fixation. Figure S18 shows the effect of Cl^- concentration during the photoreaction of BiOCl-OVs in acidic solutions (pH 1.0) under N_2 flow on the NH_3 formation. The activity increases with an increase in the Cl^- concentration and becomes almost constant at >400 mM Cl^-. This clearly indicates that an acidic solution containing Cl^- at a seawater level (~550 mM) is suitable for efficient N_2 photofixation.

The performance of this system in artificial photosynthesis was studied by AM1.5G simulated sunlight (1 sun)[56] (Figure S10) and N_2 flow. Figure 2d shows the time courses for the amount of NH_3 formed and SCC efficiency. During photoirradiation in a KCl solution at pH 1.0 (square symbols), the SCC efficiency is 0.10% and remains almost constant even after prolonged photoirradiation. Table S2 summarizes the activities for N_2 fixation with water on several powder photocatalysts. To the best of our knowledge, the present BiOCl-OVs system exhibits the highest SCC efficiency among previously reported systems. In addition, as shown by the circle symbols, the use of seawater (pH 1.0), prepared by dissolving red sea salt containing ~550 mM of Cl^- in water, also stably produces NH_3, although the efficiency (~0.05%) is about half of that obtained in the KCl solution. This suggests that seawater can be used as a solvent for N_2 fixation, although it contains several impurities such as cations (Na^+, K^+, Ca^{2+}, Mg^{2+}, and Sr^{2+}) and anions (SO_4^{2-}, HCO_3^-, Br^-, and $H_2BO_3^-$).[57] In addition, these SCC efficiencies are comparable to the average efficiency of natural photosynthesis by typical plants (~0.1%).[58] Although the efficiencies are below the highest levels achieved by artificial photosynthesis by powder catalysts for overall water splitting (~0.2%, eq 4)[7−9] and H_2O_2 production (~0.5%, eq 5),[10−12] stable N_2 fixation in seawater under sunlight shows potential as a new artificial photosynthesis system.

Catalytic Mechanism. The N_2 fixation on BiOCl-OVs in acidic Cl^- solutions involves (i) reduction of N≡N to N=N on the Bi^{II} sites adjacent to the surface OVs, (ii) water oxidation via oxidation of interlayer Cl^- by the VB h^+ followed by HClO photodecomposition, and (iii) stepwise reduction of the intermediates by the CB e^- (Figure 4). As shown in a → b, N_2 is reduced on the Bi^{II} sites via electron donation, as confirmed by ESR (Figure S9). The signal assigned to the unpaired electrons of the Bi^{II} sites on BiOCl-OVs decreases upon N_2 injection, confirming that the electron transfer from Bi^{II} to N_2 creates Bi^{III} species. The behavior of N_2 on the catalysts was further studied by diffuse-reflectance infrared Fourier transform spectroscopy (DRIFTS) at 100 K. Figure 5a shows the DRIFTS charts after injection of water and N_2 into BiOCl in the dark. A band for ν(O−H) stretching of adsorbed water appears at 3608 cm^{-1}, and two absorption bands for ν(N−H) stretching and σ(N−H) bending of N_2 adsorbed on the surface −OH groups of the catalyst appear at 3441 and 1608 cm^{-1},[26,35,36] respectively, whereas only a weak band assigned to ν(N=N) stretching appears at 2103 cm^{-1}.[26] In contrast, injection of N_2 into BiOCl-OVs (Figure 5b) creates a

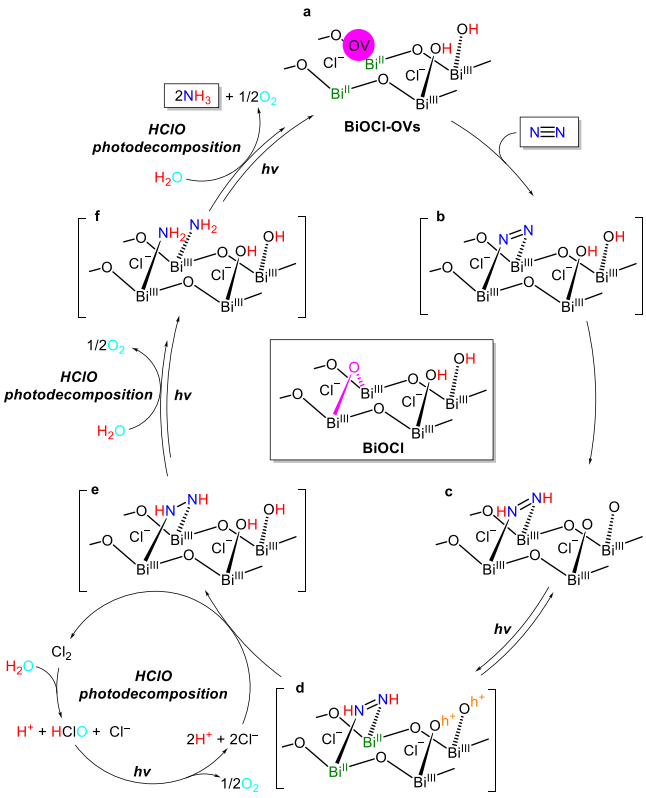

Figure 4. Proposed pathway for N_2 fixation on BiOCl-OVs in acidic Cl^- solution under photoirradiation.

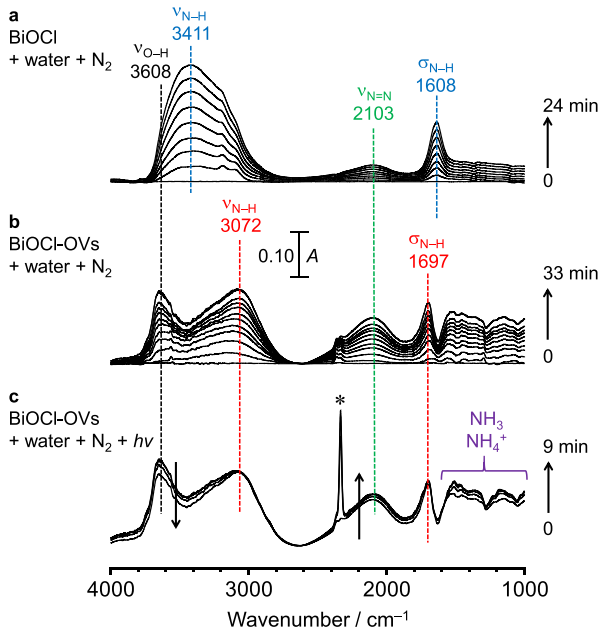

Figure 5. DRIFT charts of N_2 adsorbed on the catalysts at 100 K. Measurements were started in the dark after injection of water vapor (42 μmol) and N_2 (42 μmol) into the cell containing (a) BiOCl and (b) BiOCl-OVs (20 mg). (c) The spectrum of sample b, left for 33 min after the injection of water and N_2, was then measured under photoirradiation. The absorption band (*) at 2333 cm^{-1} in the spectrum c is assigned to the N_2 molecules chemisorbed on the Brønsted acid site formed by oxidation of interlayer Cl^- by the VB h^+ (eqs 6 and 9).[61]

https://dx.doi.org/10.1021/jacs.0c01683
J. Am. Chem. Soc. XXXX, XXX, XXX−XXX

new ν(N−H) stretching at 3072 cm^{-1} together with a new σ(N−H) bending at 1697 cm^{-1}, while the ν(N═N) stretching at 2103 cm^{-1} increases significantly. This indicates that, as shown in Figure 4a → b → c, N_2 is adsorbed on the two Bi^{II} sites in an end-on/end-on bridging mode[59,60] by electron donation from the latter to the respective N atoms, producing a N═N species (b). Fast donation of H atoms from the adjacent surface −OH to the species creates a diazene intermediate (c).

Figure 5c shows the change in the DRIFTS chart of the N_2-adsorbed BiOCl-OVs under photoirradiation. Broad absorption bands appear at 1000−1600 cm^{-1} and are attributed to the symmetric and antisymmetric deformations of NH_4^+ and NH_3.[20,36] A sharp band formed at 2333 cm^{-1} is assigned to N_2 chemisorbed on the Brønsted acid site,[61] which may be formed by oxidation of interlayer Cl^- by the VB h^+ (eqs 6 and 9). These results suggest that the N_2 adsorbed on the surface OVs is reduced to NH_3 by the CB e^-, while the VB h^+ oxidize interlayer Cl^-. As shown in Figure 4, the diazene intermediate (c) can undergo stepwise reduction and produce NH_3 and O_2 via oxidation of interlayer Cl^-, followed by photodecomposition of HClO. Photoexcitation of BiOCl-OVs with the intermediate (c) produces e^- and h^+ pairs. The CB e^- reduces the two Bi^{III} sites, regenerating them to Bi^{II} (d). The VB h^+ oxidizes interlayer Cl^-, and the photodecomposition of the HClO formed produces O_2 and regenerates Cl^-. The two Bi^{II} sites promote N═N reduction and produce a hydrazine intermediate (e). Further reduction of the strongly adsorbed intermediate may give amine intermediates (f) without formation of hydrazine in solution, finally producing NH_3 with the Bi^{II} regeneration (a). The photocatalytic sequence around the surface OVs involving photodecomposition of HClO facilitates efficient NH_3 production with water as the electron donor.

CONCLUSION

We found that ultraviolet light irradiation of the BiOCl-OVs catalyst in Cl^--containing solution (e.g., seawater) at acidic pH efficiently promotes N_2 fixation with water under ambient conditions. The surface OVs act as the sites of N_2 reduction by the CB e^-. The VB h^+ oxidize the interlayer Cl^- of the catalyst (self-oxidation). Subsequent photodecomposition of the HClO formed facilitates O_2 evolution. The Cl^- in solution compensates for the removed interlayer Cl^- and suppresses catalyst deactivation. These reactions facilitate efficient and stable N_2 fixation with water as the electron donor. The SCC efficiency of N_2 fixation in seawater is 0.05%, which is comparable to the average efficiency of natural photosynthesis in plants. This new system has several advantages: (i) naturally abundant seawater and sunlight are available, (ii) noble-metal-free photocatalyst made by facile solvothermal method can be used, and (iii) storable and transportable NH_3 solution can directly be obtained. For practical application of the present process, there is several challenging issues such as generation of pure N_2 gas from air containing a large amount of O_2, which suppresses N_2 reduction, and separation of NH_3 from seawater containing a large amount of electrolytes. Nevertheless, the new concept for N_2 fixation based on a cheap oxychloride catalyst and seawater presented herein may contribute to the design of new artificial photosynthesis systems for clean solar fuel production.

EXPERIMENTAL SECTION

Catalyst Preparation. BiOCl-OVs was prepared by a solvothermal method.[35] $Bi(NO_3)_3{\cdot}5H_2O$ (1.45 g, 3.0 mmol) and KCl (0.22 g, 3.0 mmol) were stirred in ethylene glycol (16 mL) for 30 min, and the mixture was left in an autoclave at 433 K for 12 h. The resulting powder was recovered by centrifugation, washed with water and ethanol, and dried at 353 K for 24 h. BiOCl with perfect stoichiometry was prepared in water[34] in a manner similar to that of BiOCl-OVs.

Photoreaction. The catalyst (0.2 g) and solution (0.1 L) were added to a glass tube (internal diameter, 45 mm; capacity, 0.2 L). Water, 550 mM KCl solution, or seawater was used for reactions. Seawater was prepared by dissolving 33.4 g of red sea salt in 1 L of water to form a solution containing ∼550 mM of Cl^-, and the solution pH was adjusted by adding $HClO_4$.[44] The reaction solution was stirred using a magnetic stirrer and placed under N_2 flow (0.3 L min^{-1}), and the tube was photoirradiated by a Xe lamp.[48] The solution temperature was ∼303 K during photoirradiation. For the SCC efficiency determination, the reactions were performed using a solar simulator, whose irradiance was adjusted to the AM1.5 spectrum (1 sun).[56] The efficiency was calculated using the following equation:[24]

$$\text{SCC efficiency (\%)} = \frac{[\Delta G \text{ for } NH_3 \text{ formation (J mol}^{-1})] \times [NH_3 \text{ formed (mol)}]}{[\text{total input energy (W)}] \times [\text{reaction time (s)}]} \times 100 \quad (13)$$

The total input energy was 0.314 W based on the free energy for NH_3 generation (339 kJ mol^{-1}), the irradiance at 300−2500 nm (1000 W m^{-2}),[56] and the irradiation area (3.14×10^{-4} m^2). Photographs of the flow and closed circulation systems employed for photoreactions are shown in Figures S19 and S20, respectively. After the reactions, the catalyst was recovered by centrifugation. The NH_4^+ amount in the resulting water or KCl solutions was analyzed using an ion chromatograph equipped with a conductivity detector. A 3.5 mM $(COOH)_2$ solution containing 2.0 mM 18-crown-6 ether was used as the eluent to suppress the interference by the K^+ cation.[62] The NH_4^+ amount in seawater was determined by UV−visible absorption spectroscopy after the indophenol assay.[26]

Analysis. Electrochemical measurements were carried out using 1.0 M Na_2SO_4 solution or 550 mM KCl solution with a Pt wire (counter) and a Ag/AgCl (reference) electrode. The solution pH was adjusted with H_2SO_4, and N_2 was bubbled through the solution for 10 min prior to measurements. The working electrode was prepared with a glassy carbon substrate (2 cm^2).[63] All potential values are expressed with respect to the RHE for ease of comparison of the data obtained at different pH values using the following equations:[64]

$$E(\text{vs RHE}) = E(\text{vs Ag/AgCl}) + E_{Ag/AgCl}(\text{ref}) + 0.0591V \times \text{pH}$$

$$(E_{Ag/AgCl}(\text{ref}) = 0.1976V \text{ vs NHE at 25°C}) \quad (14)$$

The DRIFTS charts were obtained using a FT-IR system with an in situ diffuse reflectance cell.[65] The catalyst (20 mg) was added to the cell, which was then evacuated (10 Pa) at 303 K for 6 h. Water vapor (42 μmol) and N_2 (42 μmol) were injected into the cell at 100 K, and measurements were started in the dark. The spectra were then monitored under photoirradiation by a Xe lamp at λ > 300 nm and 100 K. The ESR spectra were recorded on the Bruker EMX-10/12 spectrometer.[66] The catalyst (20 mg) was added to a quartz tube, which was evacuated at 298 K for 6 h, and analyzed at 77 K. N_2 (20 Torr) was added to the tube at 298 K and left for 6 h, and the tube was analyzed at 77 K. The instruments and procedures used for the DR UV−visible spectroscopy, XRD, XPS, and SEM measurements are described in our previous work.[67]

https://dx.doi.org/10.1021/jacs.0c01683
J. Am. Chem. Soc. XXXX, XXX, XXX−XXX

■ ASSOCIATED CONTENT

Supporting Information

The Supporting Information is available free of charge at https://pubs.acs.org/doi/10.1021/jacs.0c01683.

SEM images (Figure S1), N_2 adsorption/desorption isotherms (S2), DR UV−vis spectra (S3), electrochemical Mott−Schottky plots (S4), XRD (S5), XPS at Bi 4f (S6), O 1s (S7), and Cl 2p levels (S8), ESR (S9), light emission spectra (S10), absorption spectra of the solution after photoreaction (S11), NH_3 decomposition by HClO (S12), isotopic labeling experiments (S13), O_2 evolution by HClO photodecomposition (S14), absorption spectra of the solution after photoreaction followed by DPD assay (S15), NH_3 and HClO formation (S16), photographs of the solution containing catalyst (S17), effect of Cl^- concentration on the NH_3 formation (S18), flow photoreactor (S19), and closed circulation photoreactor (S20), results of photocatalytic NH_3 formation (Table S1), SCC efficiencies in literature (S2), and references (PDF)

■ AUTHOR INFORMATION

Corresponding Author

Yasuhiro Shiraishi − *Research Center for Solar Energy Chemistry, and Division of Chemical Engineering, Graduate School of Engineering Science, Osaka University, Toyonaka 560-8531, Japan;* orcid.org/0000-0003-1812-0644; Email: shiraish@cheng.es.osaka-u.ac.jp

Authors

Masaki Hashimoto − *Research Center for Solar Energy Chemistry, and Division of Chemical Engineering, Graduate School of Engineering Science, Osaka University, Toyonaka 560-8531, Japan*

Kiyomichi Chishiro − *Research Center for Solar Energy Chemistry, and Division of Chemical Engineering, Graduate School of Engineering Science, Osaka University, Toyonaka 560-8531, Japan*

Kenta Moriyama − *Research Center for Solar Energy Chemistry, and Division of Chemical Engineering, Graduate School of Engineering Science, Osaka University, Toyonaka 560-8531, Japan*

Shunsuke Tanaka − *Department of Chemical, Energy, and Environmental Engineering, Kansai University, Suita 564-8680, Japan;* orcid.org/0000-0001-5157-3317

Takayuki Hirai − *Research Center for Solar Energy Chemistry, and Division of Chemical Engineering, Graduate School of Engineering Science, Osaka University, Toyonaka 560-8531, Japan*

Complete contact information is available at: https://pubs.acs.org/10.1021/jacs.0c01683

Author Contributions

The manuscript was written by Y.S. through the contributions of all authors.

Notes

The authors declare no competing financial interest.

■ ACKNOWLEDGMENTS

This work was supported by the Precursory Research for Embryonic Science and Technology (PRESTO, JPMJPR1442) program of the Japan Science and Technology Agency (JST) and the Grant-in-Aid for Scientific Research (no. 19H02516) from the Ministry of Education, Culture, Sports, Science and Technology, Japan (MEXT).

■ REFERENCES

(1) Smil, V. Detonator of the population explosion. *Nature* **1999**, *400*, 415−415.

(2) Klerke, A.; Christensen, C. H.; Nørskov, J. K.; Vegge, T. Ammonia for hydrogen storage: challenges and opportunities. *J. Mater. Chem.* **2008**, *18*, 2304−2310.

(3) Lan, R.; Tao, S. Direct ammonia alkaline anion-exchange membrane fuel cells. *Electrochem. Solid-State Lett.* **2010**, *13*, B83.

(4) Aika, K.; Chiristiansen, L. J.; Dybkjacr, I.; Hansen, J. B.; Nielsen, H.; Nielsen, A.; Stoltze, P.; Tamaru, K. *Catalysis and Manufacture*; Springer-Verlag: Heidelberg, 1995.

(5) Medford, A. J.; Hatzell, M. C. Photon-Driven Nitrogen Fixation: Current Progress, Thermodynamic Considerations, and Future Outlook. *ACS Catal.* **2017**, *7*, 2624−2643.

(6) Thacker, C. M.; Folkins, H. O.; Miller, E. L. Free energies of formation of gaseous hydrocarbons and related substances. *Ind. Eng. Chem.* **1941**, *33*, 584.

(7) Maeda, K.; Teramura, K.; Lu, D.; Takata, T.; Saito, N.; Inoue, Y.; Domen, K. Photocatalyst Releasing Hydrogen from Water. *Nature* **2006**, *440*, 295.

(8) Kubota, J.; Domen, K. Photocatalytic Water Splitting Using Oxynitride and Nitride Semiconductor Powders for Production of Solar Hydrogen. *Electrochem. Soc. Interface* **2013**, *22*, 57−62.

(9) Sasaki, Y.; Nemoto, H.; Saito, K.; Kudo, A. Solar water splitting using powdered photocatalysts driven by Z-schematic interparticle electron transfer without an electron mediator. *J. Phys. Chem. C* **2009**, *113*, 17536−17542.

(10) Shiraishi, Y.; Kanazawa, S.; Kofuji, Y.; Sakamoto, H.; Ichikawa, S.; Tanaka, S.; Hirai, T. Sunlight-Driven Hydrogen Peroxide Production from Water and Molecular Oxygen by Metal-Free Photocatalysts. *Angew. Chem., Int. Ed.* **2014**, *53*, 13454−13459.

(11) Kofuji, Y.; Isobe, Y.; Shiraishi, Y.; Sakamoto, H.; Tanaka, S.; Ichikawa, S.; Hirai, T. Carbon Nitride-Aromatic Diimide-Graphene Nanohybrids: Metal-Free Photocatalysts for Solar-to-Hydrogen Peroxide Energy Conversion with 0.2% Efficiency. *J. Am. Chem. Soc.* **2016**, *138*, 10019−10025.

(12) Shiraishi, Y.; Takii, T.; Hagi, T.; Mori, S.; Kofuji, Y.; Kitagawa, Y.; Tanaka, S.; Ichikawa, S.; Hirai, T. Resorcinol-Formaldehyde Resins as Metal-Free Semiconductor Photocatalysts for Solar-to-Hydrogen Peroxide Energy Conversion. *Nat. Mater.* **2019**, *18*, 985−993.

(13) Schrauzer, G. N.; Guth, T. D. Photolysis of water and photoreduction of nitrogen on titanium dioxide. *J. Am. Chem. Soc.* **1977**, *99*, 7189−7193.

(14) Chen, X.; Li, N.; Kong, Z.; Ong, W. J.; Zhao, X. Photocatalytic fixation of nitrogen to ammonia: State-of-the-art advancements and future prospects. *Mater. Horiz.* **2018**, *5*, 9−27.

(15) Oshikiri, T.; Ueno, K.; Misawa, H. Plasmon-induced ammonia synthesis through nitrogen photofixation with visible light irradiation. *Angew. Chem., Int. Ed.* **2014**, *53*, 9802−9805.

(16) Xiao, C.; Hu, H.; Zhang, X.; MacFarlane, D. R. Nanostructured Gold/Bismutite Hybrid Heterocatalysts for Plasmon-Enhanced Photosynthesis of Ammonia. *ACS Sustainable Chem. Eng.* **2017**, *5*, 10858−10863.

(17) Hao, Y.; Dong, X.; Zhai, S.; Ma, H.; Wang, X.; Zhang, X. Hydrogenated Bismuth Molybdate Nanoframe for Efficient Sunlight-Driven Nitrogen Fixation from Air. *Chem. - Eur. J.* **2016**, *22*, 18722−18728.

(18) Sun, X.; Jiang, D.; Zhang, L.; Sun, S.; Wang, W. Enhanced nitrogen photofixation over $LaFeO_3$ via acid Treatment. *ACS Sustainable Chem. Eng.* **2017**, *5*, 9965−9971.

(19) Zhang, N.; Jalil, A.; Wu, D.; Chen, S.; Liu, Y.; Gao, C.; Ye, W.; Qi, Z.; Ju, H.; Wang, C.; Wu, X.; Song, L.; Zhu, J.; Xiong, Y. Refining Defect States in $W_{18}O_{49}$ by Mo Doping: A Strategy for Tuning N_2

Activation towards Solar-Driven Nitrogen Fixation. *J. Am. Chem. Soc.* **2018**, *140*, 9434−9443.
(20) Zhao, Y.; Zhao, Y.; Waterhouse, G. I. N.; Zheng, L.; Cao, X.; Teng, F.; Wu, L. Z.; Tung, C. H.; O'Hare, D.; Zhang, T. Layered-Double-Hydroxide Nanosheets as Efficient Visible-Light-Driven Photocatalysts for Dinitrogen Fixation. *Adv. Mater.* **2017**, *29*, 1703828.
(21) Sun, S.; Li, X.; Wang, W.; Zhang, L.; Sun, X. Photocatalytic robust solar energy reduction of dinitrogen to ammonia on ultrathin MoS_2. *Appl. Catal., B* **2017**, *200*, 323−329.
(22) Banerjee, A.; Yuhas, B. D.; Margulies, E. A.; Zhang, Y.; Shim, Y.; Wasielewski, M. R.; Kanatzidis, M. G. Photochemical Nitrogen Conversion to Ammonia in Ambient Conditions with Femos-Chalcogels. *J. Am. Chem. Soc.* **2015**, *137*, 2030−2034.
(23) Li, X.; Wang, W.; Jiang, D.; Sun, S.; Zhang, L.; Sun, X. Efficient Solar-Driven Nitrogen Fixation over Carbon−Tungstic-Acid Hybrids. *Chem. - Eur. J.* **2016**, *22*, 13819−13822.
(24) Shiraishi, Y.; Shiota, S.; Kofuji, Y.; Hashimoto, M.; Chishiro, K.; Hirakawa, H.; Tanaka, S.; Ichikawa, S.; Hirai, T. Nitrogen Fixation with Water on Carbon-Nitride-Based Metal-Free Photocatalysts with 0.1% Solar-to-Ammonia Energy Conversion Efficiency. *ACS Appl. Energy Mater.* **2018**, *1*, 4169−4177.
(25) Li, X. H.; Chen, W. L.; Tan, H. Q.; Li, F. R.; Li, J. P.; Li, Y. G.; Wang, E. B. Reduced State of the Graphene Oxide@Polyoxometalate Nanocatalyst Achieving High-Efficiency Nitrogen Fixation under Light Driving Conditions. *ACS Appl. Mater. Interfaces* **2019**, *11*, 37927−37938.
(26) Hirakawa, H.; Hashimoto, M.; Shiraishi, Y.; Hirai, T. Photocatalytic conversion of nitrogen to ammonia with water on surface oxygen vacancies of titanium dioxide. *J. Am. Chem. Soc.* **2017**, *139*, 10929−10936.
(27) Comer, B. M.; Medford, A. J. Analysis of Photocatalytic Nitrogen Fixation on Rutile TiO_2(110). *ACS Sustainable Chem. Eng.* **2018**, *6*, 4648−4660.
(28) Comer, B. M.; Liu, Y. H.; Dixit, M. B.; Hatzell, K. B.; Ye, Y.; Crumlin, E. J.; Hatzell, M. C.; Medford, A. J. The Role of Adventitious Carbon in Photo-Catalytic Nitrogen Fixation by Titania. *J. Am. Chem. Soc.* **2018**, *140*, 15157−15160.
(29) Hisatomi, T.; Kubota, J.; Domen, K. Recent advances in semiconductors for photocatalytic and photoelectrochemical water splitting. *Chem. Soc. Rev.* **2014**, *43*, 7520−7535.
(30) Kudo, A.; Miseki, Y. Heterogeneous photocatalyst materials for water splitting. *Chem. Soc. Rev.* **2009**, *38*, 253−278.
(31) Ye, L.; Su, Y.; Jin, X.; Xie, H.; Zhang, C. Recent advances in BiOX (X = Cl, Br and I) photocatalysts: synthesis, modification, facet effects and mechanisms. *Environ. Sci.: Nano* **2014**, *1*, 90−112.
(32) Li, J.; Yu, Y.; Zhang, L. Bismuth oxyhalide nanomaterials: layered structures meet photocatalysis. *Nanoscale* **2014**, *6*, 8473−8488.
(33) Li, H.; Li, J.; Ai, Z.; Jia, F.; Zhang, L. Oxygen Vacancy-Mediated Photocatalysis of BiOCl: Reactivity, Selectivity, and Perspectives. *Angew. Chem., Int. Ed.* **2018**, *57*, 122−138.
(34) Li, H.; Shang, J.; Shi, J.; Zhao, K.; Zhang, L. Facet-Dependent Solar Ammonia Synthesis of BiOCl Nanosheets via a Proton-Assisted Electron Transfer Pathway. *Nanoscale* **2016**, *8*, 1986−1993.
(35) Li, H.; Shang, J.; Ai, Z.; Zhang, L. Efficient Visible Light Nitrogen Fixation with BiOBr Nanosheets of Oxygen Vacancies on the Exposed {001} Facets. *J. Am. Chem. Soc.* **2015**, *137*, 6393−6399.
(36) Bai, Y.; Ye, L.; Chen, T.; Wang, L.; Shi, X.; Zhang, X.; Chen, D. Facet-Dependent Photocatalytic N_2 Fixation of Bismuth-Rich Bi_5O_7I Nanosheets. *ACS Appl. Mater. Interfaces* **2016**, *8*, 27661−27668.
(37) Wang, S.; Hai, X.; Ding, X.; Chang, K.; Xiang, Y.; Meng, X.; Yang, Z.; Chen, H.; Ye, J. Light-Switchable Oxygen Vacancies in Ultrafine Bi_5O_7Br Nanotubes for Boosting Solar-Driven Nitrogen Fixation in Pure Water. *Adv. Mater.* **2017**, *29*, 1701774.
(38) Fujito, H.; Kunioku, H.; Kato, D.; Suzuki, H.; Higashi, M.; Kageyama, H.; Abe, R. Layered perovskite oxychloride Bi_4NbO_8Cl: a stable visible light responsive photocatalyst for water splitting. *J. Am. Chem. Soc.* **2016**, *138*, 2082−2085.
(39) Wu, D.; Ye, L.; Yue, S.; Wang, B.; Wang, W.; Yip, H. Y.; Wong, P. K. Alkali-Induced in Situ Fabrication of Bi_2O_4-Decorated BiOBr Nanosheets with Excellent Photocatalytic Performance. *J. Phys. Chem. C* **2016**, *120*, 7715−7727.
(40) Poznyak, S. K.; Kulak, A. I. Photoelectrochemical properties of bismuth oxyhalide films. *Electrochim. Acta* **1990**, *35*, 1941−1947.
(41) Nakagawara, S.; Goto, T.; Nara, M.; Ozawa, Y.; Hotta, K.; Arata, Y. Spectroscopic Characterization and the pH Dependence of Bactericidal Activity of the Aqueous Chlorine Solution. *Anal. Sci.* **1998**, *14*, 691−698.
(42) Watts, M. J.; Linden, K. G. Chlorine photolysis and subsequent OH radical production during UV treatment of chlorinated water. *Water Res.* **2007**, *41*, 2871−2878.
(43) Huang, L.; Li, R.; Chong, R.; Liu, G.; Han, J.; Li, C. Cl^- Making Overall Water Splitting Possible on TiO_2-Based Photocatalysts. *Catal. Sci. Technol.* **2014**, *4*, 2913−2918.
(44) Mase, K.; Yoneda, M.; Yamada, Y.; Fukuzumi, S. Seawater usable for production and consumption of hydrogen peroxide as a solar fuel. *Nat. Commun.* **2016**, *7*, 11470.
(45) Wu, S.; Xiong, J.; Sun, J.; Hood, Z. D.; Zeng, W.; Yang, Z.; Gu, L.; Zhang, X.; Yang, S. Z. Hydroxyl-Dependent Evolution of Oxygen Vacancies Enables the Regeneration of BiOCl Photocatalyst. *ACS Appl. Mater. Interfaces* **2017**, *9*, 16620−16626.
(46) Bai, L.; Ye, F.; Li, L.; Lu, J.; Zhong, S.; Bai, S. Facet Engineered Interface Design of Plasmonic Metal and Cocatalyst on BiOCl Nanoplates for Enhanced Visible Photocatalytic Oxygen Evolution. *Small* **2017**, *13*, 1701607.
(47) Wagner, C. D.; Davis, L. E.; Zeller, M. V.; Taylor, J. A.; Raymond, R. H.; Gale, L. H. Empirical Atomic Sensitivity Factors for Quantitative Analysis by Electron Spectroscopy for Chemical Analysis. *Surf. Interface Anal.* **1981**, *3*, 211−225.
(48) Shiraishi, Y.; Sugano, Y.; Tanaka, T.; Hirai, T. One-pot synthesis of benzimidazoles by simultaneous photocatalytic and catalytic reactions on Pt@TiO_2 nanoparticles. *Angew. Chem., Int. Ed.* **2010**, *49*, 1656−1660.
(49) Stumm, W.; Morgan, J. J. *Aquatic Chemistry: Chemical Equilibria and Rates in Natural Waters*, 3rd ed.; John Wiley & Sons: New York, 1996.
(50) Fujishima, Y.; Okamoto, S.; Yoshiba, M.; Itoi, T.; Kawamura, S.; Yoshida, Y.; Ogura, Y.; Izumi, Y. Photofuel Cell Comprising Titanium Oxide and Bismuth Oxychloride ($BiO_{1-x}Cl_{1-y}$) Photocatalysts That Uses Acidic Water as a Fuel. *J. Mater. Chem. A* **2015**, *3*, 8389−8404.
(51) Ma, H.; Zhao, M.; Xing, H.; Fu, Y.; Zhang, X.; Dong, X. Synthesis and Enhanced Photoreactivity of Metallic Bi-Decorated BiOBr Composites with Abundant Oxygen Vacancies. *J. Mater. Sci.: Mater. Electron.* **2015**, *26*, 10002−10011.
(52) Watt, G. W.; Chrisp, J. D. Spectrophotometric method for determination of hydrazine. *Anal. Chem.* **1952**, *24*, 2006−2008.
(53) Iguchi, S.; Teramura, K.; Hosokawa, S.; Tanaka, T. Effect of the chloride ion as a hole scavenger on the photocatalytic conversion of CO_2 in an aqueous solution over Ni-Al layered double hydroxides. *Phys. Chem. Chem. Phys.* **2015**, *17*, 17995−18003.
(54) Du, J.; Chen, Z.; Chen, C.; Meyer, T. J. A Half-Reaction Alternative to Water Oxidation: Chloride Oxidation to Chlorine Catalyzed by Silver Ion. *J. Am. Chem. Soc.* **2015**, *137*, 3193−3196.
(55) Noyes, A. A.; Hall, F. M.; Beattie, J. A. The solubility of bismuth oxychloride in hydrochloric acid and its relation to complex formation. *J. Am. Chem. Soc.* **1917**, *39*, 2526−2532.
(56) Gordon, I.; Krebs, F. C.; Mathew, X.; Lampert, C. M.; Rougier, A.; Smestad, G. P.; Subrahmanyam, A. Editorial. *Sol. Energy Mater. Sol. Cells* **2015**, *133*, A1−A6.
(57) Hill, M. N. *The composition of sea-water; Comparative and descriptive oceanography*; Interscience: New York, 1963.
(58) Reijnders, L.; Huijbregts, M. *Biofuels for Road Transport: A Seed to Wheel Perspective*; Springer: New York, 2009.
(59) Holland, P. L. Metal−dioxygen and metal−dinitrogen complexes: where are the electrons? *Dalton Trans.* **2010**, *39*, 5415−5425.

https://dx.doi.org/10.1021/jacs.0c01683
J. Am. Chem. Soc. XXXX, XXX, XXX−XXX

(60) Hinrichsen, S.; Broda, H.; Gradert, C.; Söncksen, L.; Tuczek, F. Recent developments in synthetic nitrogen fixation. *Annu. Rep. Prog. Chem., Sect. A: Inorg. Chem.* **2012**, *108*, 17−47.
(61) Wakabayashi, F.; Kondo, J.; Domen, K.; Hirose, C. Does the IR spectroscopic result of $^{14}N^{15}N$ adsorption on H-form zeolites mean the side-on type adsorption of the N_2 species? *Microporous Mater.* **1993**, *2*, 35−39.
(62) Kawase, I.; Lim, L. W.; Takeuchi, T. Capillary Ion Chromatography Using 18-Crown-6 Ether as Eluent Additive for the Separation of Anions. *Chromatographia* **2017**, *80*, 1089−1093.
(63) Fellinger, T. P.; Hasché, F.; Strasser, P.; Antonietti, M. Mesoporous Nitrogen-Doped Carbon for the Electrocatalytic Synthesis of Hydrogen Peroxide. *J. Am. Chem. Soc.* **2012**, *134*, 4072−4075.
(64) Seabold, J. A.; Choi, K. S. Efficient and stable photo-oxidation of water by a bismuth vanadate photoanode coupled with an iron oxyhydroxide oxygen evolution catalyst. *J. Am. Chem. Soc.* **2012**, *134*, 2186−2192.
(65) Sakamoto, H.; Ohara, T.; Yasumoto, N.; Shiraishi, Y.; Ichikawa, S.; Tanaka, S.; Hirai, T. Hot-Electron-Induced Highly Efficient O_2 Activation by Pt Nanoparticles Supported on Ta_2O_5 Driven by Visible Light. *J. Am. Chem. Soc.* **2015**, *137*, 9324−9332.
(66) Sugano, Y.; Shiraishi, Y.; Tsukamoto, D.; Ichikawa, S.; Tanaka, S.; Hirai, T. Supported Au-Cu Bimetallic Alloy Nanoparticles: An Aerobic Oxidation Catalyst with Regenerable Activity by Visible-Light Irradiation. *Angew. Chem., Int. Ed.* **2013**, *52*, 5295−5299.
(67) Shiraishi, Y.; Tanaka, K.; Shirakawa, E.; Sugano, Y.; Ichikawa, S.; Tanaka, S.; Hirai, T. Light-Triggered Self-Assembly of Gold Nanoparticles Based on Photoisomerization of Spirothiopyran. *Angew. Chem., Int. Ed.* **2013**, *52*, 8304−8308.

https://dx.doi.org/10.1021/jacs.0c01683
J. Am. Chem. Soc. XXXX, XXX, XXX−XXX